An introduction to MRI, EPI, and EPTI

Kaibo Tang

March 3, 2026

1 Preliminary

The Larmor equation describes the rate of precession (in rad/s) of the magnetic moment (of ^{1}H) around an external magnetic field B:

$$\omega = \gamma B. \tag{1}$$

Here, the gyromagnetic ratio (for ^{1}H) is given by $\gamma = 2.675 \times 10^8$ rad/s/T.

The Bloch equations are an effective theory that describes the temporal evolution of nuclear magnetization (the net nuclear magnetic moment per unit volume) M under an external magnetic field B. The Bloch equations are given by

$$\frac{dM}{dt} = \gamma M \times B. \tag{2}$$

Typically, we denote by M_z the longitudinal magnetization and by M_{xy} the transverse magnetization.

A particular solution of the Bloch equations, assuming magnetic field B with only z-component, takes the following form:

$$M_{xy}(x, y, t) = M(x, y, 0) \exp(-t/T_2) \exp(-j\omega t), \tag{3}$$

where $\exp(-t/T_2)$ describes the decay (relaxation) of the transverse magnetization due to T_2-relaxation (spin–spin relaxation).

For static field B_0, we have

$$\omega = \omega_0 := \gamma B_0. \tag{4}$$

If we consider a spatiotemporally varying field $B_z(x, y, t)$ that is spatially linear and superimposed on B_0, which we characterize by its gradients

$$G_x(t) = \frac{\partial B_z(t)}{\partial x}, \quad G_y(t) = \frac{\partial B_z(t)}{\partial y}, \tag{5}$$

then the overall magnetic field is

$$B = B_0 + B_z = B_0 + xG_x(t) + yG_y(t), \tag{6}$$

in which case,

$$\omega = \gamma(B_0 + xG_x(t) + yG_y(t)) = \omega_0 + \gamma(xG_x(t) + yG_y(t)). \tag{7}$$

Suppose T_2-relaxation is negligible[1] and let $\rho(x, y) = M_{xy}(x, y, 0)$, Equation 3 becomes

$$M_{xy}(x, y, t) = \rho(x, y) \exp(-j\omega_0 t) \exp(-j\gamma(xG_x(t) + yG_y(t))). \tag{8}$$

The receiver coils of an MRI scanner measures the voltage induced by the temporally varying transverse magnetization within the object,[2] which is proportional to the spatial integral of M_{xy} over the entire field of view as a function of time, which is then demodulated to remove the $\exp(-i\omega_0 t)$ term. This integral (after demodulation) is given by

$$s(t) = \iint \rho(x, y) \exp(-j2\pi(k_x(t)x + k_y(t)y))\ dxdy, \tag{9}$$

where[3]

$$k_x(t) = \frac{\gamma}{2\pi} \int_0^t G_x(\tau)\ d\tau, \quad k_y(t) = \frac{\gamma}{2\pi} \int_0^t G_y(\tau)\ d\tau. \tag{10}$$

2 Phase and frequency encoding

Notice that Equation 9 resembles the 2D CSFT of $\rho(x, y)$. Indeed,

$$\hat{\rho}(k_x, k_y) = \iint \rho(x, y) \exp(-j2\pi(k_x x + k_y y))\ dxdy. \tag{11}$$

[1] This is not a crazy assumption, as we will see before long.

[2] Faraday's law of electromagnetic induction.

[3] The integral accounts for phase accumulation over $[0, t]$.

Hence, after discretizing $\rho(x, y)$, we can manipulate G_x and G_y to sample $\hat{\rho}(k_x, k_y)$ at appropriate locations such that $\rho(x, y)$ can be recovered by 2D IDFT. In practice, each k_y-line is sampled for all k_x before moving on to the next k_y-line.

Let $\rho[m, n]$ where $m = 0, 1, \ldots, M-1$ and $n = 0, 1, \ldots, N-1$ denote the discretized image. We refer to the space defined by (m, n) as the image space. Let $\hat{\rho}[k, \ell]$ where $k = -M/2, -M/2+1, \ldots, M/2-1$ and $l = -N/2, -N/2+1, \ldots, N/2-1$ denote its 2D DFT. We refer to the space defined by (k, ℓ) as the k-space. Furthermore, let FOV_x and FOV_y denote the field of view in x and y directions. Hence, the spacing of k-space is given by

$$\Delta k_x = \frac{1}{\mathrm{FOV}_x}, \quad \Delta k_y = \frac{1}{\mathrm{FOV}_y}. \tag{12}$$

Fix ℓ. The rest of this section describes how to sample the k_y-line indexed by ℓ, which can then be repeated to sample the entire k-space.

2.1 Phase encoding

We manipulate G_y to move to $k_y = \ell/\mathrm{FOV}_y$ before readout in the k_x direction. Doing so requires

$$\frac{\ell}{\mathrm{FOV}_y} = k_y = \frac{\gamma}{2\pi} \int_0^{\tau_y} G_y(\tau)\, d\tau. \tag{13}$$

Hence,

$$\int_0^{\tau_y} G_y(\tau)\, d\tau = \frac{2\pi}{\gamma} \frac{\ell}{\mathrm{FOV}_y}, \tag{14}$$

i.e., G_y is turned on for τ_y and then turned off before readout, which will be described in the next subsection.

2.2 Frequency encoding

After phase encoding, we turn on the G_x gradient, which stays constant during the entire readout, to traverse across all k_x locations. Hence, for fixed k, we require

$$\frac{k}{\mathrm{FOV}_x} = k_x = \frac{\gamma}{2\pi} \int_0^{\tau_x} G_x(\tau)\, d\tau = \frac{\gamma}{2\pi} G_x \tau_x. \tag{15}$$

In reality, the spacing between two consecutive τ_x is determined by the ADC dwell time Δt. Hence, we require

$$\frac{1}{\mathrm{FOV}_x} = \frac{\gamma}{2\pi} G_x \Delta t, \tag{16}$$

which gives us the required gradient

$$G_x = \frac{2\pi}{\gamma} \frac{1}{\mathrm{FOV}_x \Delta t}. \tag{17}$$

Typically, Δt is on the order of tens of microseconds, whereas T_2 is typically on the order of hundreds of milliseconds. Hence, it is reasonable to neglect T_2 decay over one readout (i.e., one k_y-line). However, this effect becomes non-negligible across different k_y-lines if multiple k_y-lines are acquired after one excitation. Regardless, many pulse sequences still neglect T_2 decay across readouts and perform reconstruction without modeling T_2 decay in the forward model. In the next section, we will use echo planar imaging as an example to illustrate the effect of disregarding T_2 decay on the reconstructed image.

3 Example

3.1 Echo planar imaging

Echo planar imaging (EPI) is a rapid MRI technique, first described by Sir Peter Mansfield in 1977 [Man77], capable of acquiring tens of 2D images within a second.[4] Figure 1 shows the timing diagram for an EPI sequence.[5] As is shown in Figure 2, following a single RF-excitation pulse, a train of blipped low-amplitude phase-encoding gradient pulses (G_φ), combined with positive and negative frequency-encoding gradient lobes (G_f), results in a zig-zag traversal of k-space (see Figure 3).[6]

The problem with EPI is that the image of interest undergoes T_2 decay (see Figure 1) during acquisition.

[4] This later earns him and Paul Lauterbur the Nobel Prize in Physiology and Medicine in 2003.

[5] More specifically, a spin echo EPI sequence.

[6] These figures are taken from https://www.cis.rit.edu/htbooks/mri/chap-8/chap-8a.htm.

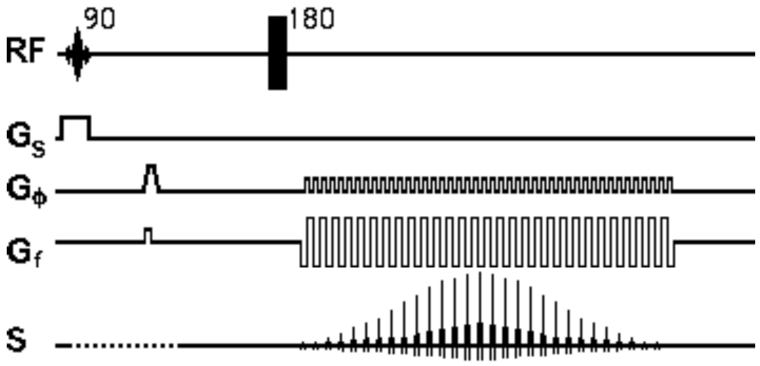

Figure 1: A timing diagram for an EPI sequence.

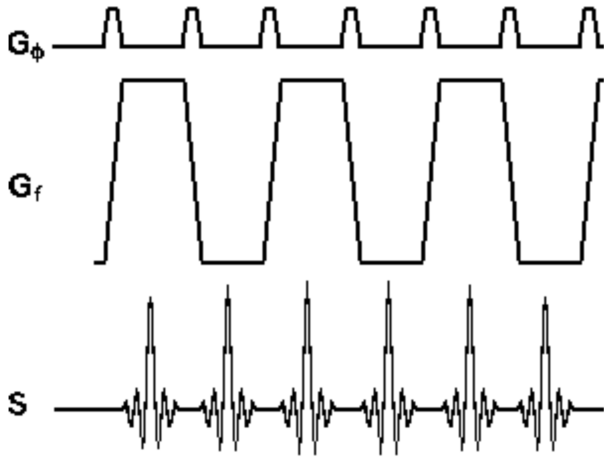

Figure 2: A zoomed-in view of the phase and frequency encoding gradients.

Consider the ideal object $\rho(x, y)$ with no T_2 decay, whose 2D CSFT is given by

$$\hat{\rho}(k_x, k_y) = \iint \rho(x, y) \exp(-j2\pi(k_x x + k_y y))\, dxdy. \tag{18}$$

EPI introduces time dependence on k_y. Let echo spacing ESP denote the time interval between the acquisition of two consecutive k_y-lines, in which case, we have

$$t = k_y \frac{\text{ESP}}{\Delta k_y}, \quad \text{i.e., } k_y = \frac{t}{\text{ESP}} \Delta k_y. \tag{19}$$

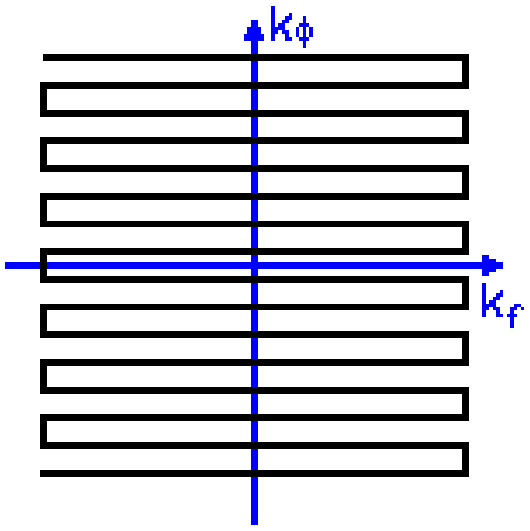

Figure 3: A zig-zag traversal of k-space.

Typically, we refer to t as the echo time (TE). For simplicity, we assume the object of interest has constant T_2, in which case, the T_2 decay (in this spin echo EPI sequence) is described by

$$\exp(-|t|/T_2) = \exp\left(-\frac{\text{ESP}}{\Delta k_y T_2}|k_y|\right) = \exp(-\alpha|k_y|) =: W(k_y). \tag{20}$$

Here, α is a constant term independent of k_y. Let $\hat{\rho}_{\text{EPI}}(k_x, k_y)$ denote the k-space data acquired using EPI, then

$$\hat{\rho}_{\text{EPI}}(k_x, k_y) = \iint \rho(x, y) W(k_y) \exp(-j2\pi(k_x x + k_y y))\, dxdy \tag{21}$$

$$= W(k_y)\hat{\rho}(k_x, k_y). \tag{22}$$

From this equation, we see that, for an object with constant T_2 acquired with EPI, the effect of neglecting T_2 decay introduces a multiplicative factor $W(k_y)$ along the k_y direction. We know multiplication in frequency domain is equivalent to convolution in the image domain, i.e.,

$$\rho_{\text{EPI}}(x, y) = \rho(x, y) * h(y) \tag{23}$$

where $*$ denotes convolution in the y direction and the point spread function

$h(y)$ is 1D IFT of $W(k_y)$, i.e.,

$$h(y) = \int_{-\infty}^{\infty} e^{-\alpha|k_y|} \exp(j2\pi k_y y)\ dk_y \tag{24}$$

$$= 2\int_{0}^{\infty} e^{-\alpha k_y} \cos(2\pi k_y y)\ dk_y \tag{25}$$

$$= 2\frac{\alpha}{\alpha^2 + (2\pi y)^2}, \tag{26}$$

where the last equality comes from consulting an integral table. See Figure 4 for a visualization of $W(k_y)$ and $h(y)$ for different α (larger T_2 corresponds to smaller α). Hence, we conclude that EPI neglects T_2 decay during acquisition, which results in blurring of the reconstructed image, which we typically refer to as T_2-blurring. Moreover, this blurring is characterized by a Lorentzian point spread function.

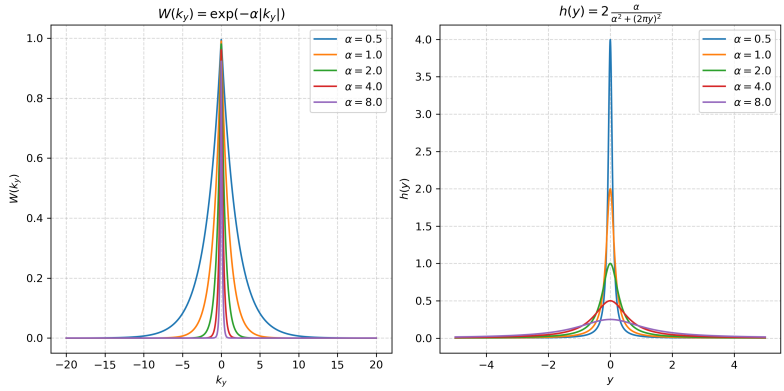

Figure 4: Visualization of $W(k_y)$ and $h(y)$ for different α.

3.2 Echo planar time-resolved imaging

It was not until recently that this issue was finally addressed by modeling T_2 decay as part of the forward model using a technique named echo planar time-resolved imaging (EPTI) [Wan+19; Don+20].[7]

Here, we present a simplified overview of EPTI in comparison to EPI. We assume the dimension of the image (and the k-space) is $N \times N$. A total

[7] This is an ongoing effort that I am proud to be a part of.

of T echoes,[8] i.e., T k_y-lines, are acquired after one RF-excitation. Finally, we assume the k-space is undersampled by acquiring M out of N^2 possible k-space samples.

The forward model of EPI (simplified, assuming a single receiver coil) is given by

$$y = UFx + \varepsilon, \quad \varepsilon \sim \mathcal{CN}(0, \sigma^2 I), \tag{27}$$

where $x \in \mathbb{C}^{N^2 \times 1}$ is the desired image to be reconstructed, $F \in \mathbb{C}^{N^2 \times N^2}$ is the 2D DFT matrix, and $U \in \{0,1\}^{M \times N^2}$ is the undersampling matrix. And $y \in \mathbb{C}^{M \times 1}$ denotes the possibly noisy observation corrupted by additive white complex Gaussian noise $\varepsilon \in \mathbb{C}^{M \times 1}$.

EPTI aims to resolve the images at each possible TE (hence the name time-resolved imaging) such that the reconstructed images are free from T_2-blurring. Doing so naively with EPI would require acquiring T times the amount of k-space data, and the number of unknowns is now $N^2 \times T$ as opposed to N^2.

The key observation that makes EPTI possible is that the space of all possible temporal evolutions of the signal at each pixel is governed by only a few physical parameters and can be very well approximated by a low-dimensional, say K-dimensional, linear subspace of $\mathbb{C}^T$ where $K \ll T$ [Lia07]. Hence, instead of reconstructing images for all possible TE by solving for $N^2 \times T$ unknowns where the feasible set is the entire $\mathbb{C}^{N^2 T \times 1}$, EPTI restricts the feasible set to an explicitly modeled low-dimensional subspace of $\mathbb{C}^{N^2 T \times 1}$, which we will make concrete in the following paragraph.

3.2.1 Explicit subspace modeling

First, a dictionary $X \in \mathbb{C}^{N_0 \times T}$ is constructed, which contains N_0 possible signal evolutions simulated using a reasonably accurate physical model.[9] Then, singular value decomposition is used to extract the K most significant right singular vectors $\Phi \in \mathbb{C}^{T \times K}$ that explain a good proportion of variance in the dictionary. Then, during reconstruction, instead of directly estimating the images $x \in \mathbb{C}^{N^2 T \times 1}$, we estimate the coefficient maps $c \in \mathbb{C}^{N^2 K \times 1}$ with respect to the estimated basis $\Phi \in \mathbb{C}^{T \times K}$. The images can then be recovered as $x = \Phi c$.

[8] Also known as echo train length (ETL).

[9] In this case, the extended phase graph [Wei15] is used, which is a framework that describes the magnetization responses of a variety of MR sequences.

3.2.2 Forward model of EPTI

The forward model (stacked appropriately) of EPTI is given by

$$y = UF\Phi c + \varepsilon, \quad \varepsilon \sim \mathcal{CN}(0, \sigma^2 I), \tag{28}$$

where $c \in \mathbb{C}^{N^2K \times 1}$ are the coefficient maps, $\Phi \in \mathbb{C}^{N^2T \times N^2K}$ is the stacked subspace basis, $F \in \mathbb{C}^{N^2T \times N^2T}$ is the stacked 2D DFT matrix, and $U \in \{0,1\}^{MT \times N^2T}$ is the undersampling matrix.[10] And $y \in \mathbb{C}^{MT \times 1}$ denotes the possibly noisy observation corrupted by additive white complex Gaussian noise $\varepsilon \in \mathbb{C}^{MT \times 1}$.

3.2.3 Reconstruction

The subspace-based reconstruction of EPTI solves the following problem

$$\min_c \|y - UF\Phi c\|_2^2 + R(c), \tag{29}$$

where $R(\cdot) : \mathbb{C}^{N^2K \times 1} \to \mathbb{R}$ is an appropriately chosen regularization term. The choice of regularization can be highly flexible, including conventional approaches (e.g., locally low-rank [LLR], total variation [TV], wavelet) or plug-and-play priors [CWE16].

In practice, the subspace-based reconstruction of EPTI is implemented with LLR as the regularization, which solves the following problem:

$$\min_c \|y - Ac\|_2^2 + \lambda \sum_{p \in P} \|R_p(C)\|_*, \tag{30}$$

where $A = UF\Phi$ is the forward operator, $C \in \mathbb{C}^{N \times N \times K}$ denotes the coefficient maps, $R_p(\cdot) : \mathbb{C}^{N \times N \times K} \to \mathbb{C}^{n \times K}$ extracts a local spatial patch with n pixel across K coefficient maps, and $\|\cdot\|_*$ denotes the nuclear norm (i.e., sum of the singular values). By introducing auxiliary variable $Z_p = R_p(C)$, the problem in Equation 30 is solved using alternating direction method of multipliers (ADMM):

[10] In practice, the matrices F and U are highly sparse and are never stored in memory during reconstruction. For example, MATLAB's `LSQR` allows the user to implement the forward and adjoint operators as functions without having to build the entire matrix. This also allows FFT to be used to implement the DFT.

1. (c-update).

$$c^{(k+1)} = \arg\min_{c} \|y - Ac\|_2^2 + \frac{\rho}{2} \sum_{p \in P} \|R_p(C) - (Z_p^{(k)} - U_p^{(k)})\|_F^2, \quad (31)$$

which is a quadratic problem that can be readily solved using conjugate gradient.

2. (Z_p-update). For each $p \in P$,

$$Z_p^{(k+1)} = \arg\min_{Z} \lambda \|Z\|_* + \frac{\rho}{2} \|Z - (R_p(C^{(k+1)} + U_p^{(k)})\|_F^2, \quad (32)$$

whose unique solution is given by singular value thresholding, i.e.,

$$Z_p^{(k+1)} = U \operatorname{diag}((\sigma_i - \lambda/\rho)_+) V^H, \quad (33)$$

where

$$R_p(C^{(k+1)}) + U_p^{(k)} = U \operatorname{diag}(\sigma_i) V^H, \quad (34)$$

is the singular value decomposition of $R_p(C^{(k+1)}) + U_p^{(k)}$.

3. (Dual update).

$$U_p^{(k+1)} = U_p^{(k)} + R_p(C^{(k+1)}) - Z_p^{(k+1)}. \quad (35)$$

References

[CWE16] Stanley H. Chan, Xiran Wang, and Omar A. Elgendy. *Plug-and-Play ADMM for Image Restoration: Fixed Point Convergence and Applications*. arXiv:1605.01710 [cs]. Nov. 2016. DOI: 10.48550/arXiv.1605.01710. URL: http://arxiv.org/abs/1605.01710 (visited on 03/02/2026).

[Don+20] Zijing Dong et al. "Echo planar time-resolved imaging with subspace reconstruction and optimized spatiotemporal encoding". en. In: *Magnetic Resonance in Medicine* 84.5 (2020), pp. 2442–2455. ISSN: 1522-2594. DOI: 10.1002/mrm.28295. URL: https://onlinelibrary.wiley.com/doi/abs/10.1002/mrm.28295 (visited on 02/12/2026).

[Lia07] Zhi-Pei Liang. "Spatiotemporal Imaging with Partially Separable Functions". In: *2007 4th IEEE International Symposium on Biomedical Imaging: From Nano to Macro*. ISSN: 1945-8452. Apr. 2007, pp. 988–991. DOI: 10.1109/ISBI.2007.357020. URL: https://ieeexplore.ieee.org/abstract/document/4193454 (visited on 02/12/2026).

[Man77] P. Mansfield. "Multi-planar image formation using NMR spin echoes". en. In: *Journal of Physics C: Solid State Physics* 10.3 (Feb. 1977), p. L55. ISSN: 0022-3719. DOI: 10.1088/0022-3719/10/3/004. URL: https://doi.org/10.1088/0022-3719/10/3/004 (visited on 03/02/2026).

[Wan+19] Fuyixue Wang et al. "Echo planar time-resolved imaging (EPTI)". en. In: *Magnetic Resonance in Medicine* 81.6 (2019), pp. 3599–3615. ISSN: 1522-2594. DOI: 10.1002/mrm.27673. URL: https://onlinelibrary.wiley.com/doi/abs/10.1002/mrm.27673 (visited on 03/02/2026).

[Wei15] Matthias Weigel. "Extended phase graphs: Dephasing, RF pulses, and echoes - pure and simple". en. In: *Journal of Magnetic Resonance Imaging* 41.2 (2015), pp. 266–295. ISSN: 1522-2586. DOI: 10.1002/jmri.24619. URL: https://onlinelibrary.wiley.com/doi/abs/10.1002/jmri.24619 (visited on 02/12/2026).